14B.8

# QUALITATIVE EVALUATION OF THE KMA REGIONAL MODEL MIXING-DEPTH PREDICTION USING WIND-PROFILER SIGNAL-TO-NOISE-RATIO DATA


Seung-Jae Lee[1*], Hee-Dong Yoo[2] and Hideaki Kawai[3]

[1] NCEP/Environmental Meteorological Center, Camp Springs, Maryland

[2] KMA/Numerical Weather Prediction Division, Seoul, Korea

[3] JMA/Climate Prediction Division, Tokyo, Japan


## 1. INTRODUCTION

Boundary layers are present when a geophysical fluid flow encounters a boundary where the fluid velocity must go to zero. In particular, over high pressure regions in the land surface an atmospheric (or planetary) boundary layer (ABL or PBL) shows a definite structure varying with the diurnal cycle (Stull 1988). The main features of the structure include a mixed layer (ML), a residual layer (RL) and a stable boundary layer (SBL). A turbulent ML begins to grow in depth about half an hour after sunrise and reaches its maximum in late afternoon. This daytime ML is usually composed of convectively driven turbulences that create thermals of warm air rising from the ground.

The concentration of atmospheric pollutants near the surface strongly depends on the development of a ML. Pollution can be transported and dispersed under stable conditions, and in fact, a great deal of horizontal pollution transport occurs at night (Gupta *et al.* 1997). However, a ML plays a distinctively significant role in most cases of vertical atmospheric contamination. For example, $CO_2$ concentration becomes higher near the ground surface after nightfall from the respiration of vegetation during the night. This is due to the formation of a SBL by the radiative cooling of the ground. The concentration continues to rise until dawn. After sunrise, the high concentration is attenuated rapidly by the development of a ML (Yi *et al*. 2001). Seasonal variations of ground-level $SO_2$ concentration, observed as low in summer and high in winter, are also related to the development of a ML. Most $SO_2$ is artificially created and discharged near the ground surface. Niisoe and Kida (2000) guessed that $SO_2$ generated near the surface is more effectively transported to the free atmosphere in summer, when a ML is well developed, than in winter.

For a precise forecast of $SO_2$, it is significantly important to understand and predict accurate height variations of a ML. There was a good case which showed the importance of knowing the height of the ML accurately. In July 2000, a volcano in Miyake Island (783 m high) erupted and released a huge amount of $SO_2$. Because of the expected impact of a particularly nasty smell on some areas and large cities in Japan, JMA (Japan Meteorological Agency) operationally predicted and announced the flow of the gas. JMA made accurate predictions because the accuracy of winds from their numerical prediction model was high (Kawai 2002). A serious uncertainty was whether the upper air flow of $SO_2$, which was almost horizontally transported by winds at the top of volcano, would reach the surface or not. Numerical simulations by Nagai *et al.* (2001) showed that $SO_2$ is brought to the surface when the top of the ML reaches the bottom of $SO_2$ layer at a height of about 700 m.

A ML is also important from the viewpoint of numerical weather prediction (NWP) due to its function to transport momentum, heat and water vapor between the surface and the free atmosphere. For instance, lots of attention has been paid to the relationship between a ML and convection. Hong and Pan (1998) took advantage of the ML height as a parameter for a trigger function for convection in a cumulus parameterization scheme. And Hong and Pan (1996) argued that in numerical atmospheric models, efforts to improve the surface and boundary layer formulation may be as important as efforts to improve the precipitation parameterizations and should be a prerequisite to realizing better precipitation forecasts.

In Japan, a Wind Profiler Network and Data Acquisition System (WINDAS) has been in operation since April 2001. Continuously observed data from wind profilers at 31 locations are available now. The KMA (Korea Meteorological Administration) also started operating two


[*] *Corresponding author address*: Seung-Jae Lee, Numerical Weather Prediction Division, Korea Meteorological Administration, 60-18 Shindaebang-dong, Dongjak-gu, Seoul, 156-720, Republic of Korea; e-mail: sjlee@kma.go.kr

additional UHF wind profilers at Munsan and Gangneung in January 2004. Each is mounted in a strategic location where the atmosphere can be observed most effectively (Fig. 1). Although the main purpose of a wind profiler is to calculate wind velocities from the Doppler velocities of fluctuations in the atmospheric refractive index caused by turbulence, it is possible that a ML height can be estimated from the reflection intensity. The ML height can be estimated from a daily radiosonde observation, but detailed time sequential information about the formation and decay of a ML cannot be obtained from low time-resolution (two or four times a day) data. Wind profilers gather data every ten minutes without any temporal break, providing more detailed information about the generation or collapse of a ML.


Figure 1. Wind profiler sites where SNR data are produced on operational basis in Korea and Japan.

Up to now, many observational or technical studies of ABLs have been conducted using wind profilers (e.g., Rogers *et al.* 1993; Lemone *et al*. 1999; Campistron *et al*. 2002; Angevine *et al*. 2001; Bianco and Wilczak 2002; Heo *et al*. 2003). Observational study of the spatio-temporal distributions and characteristics of ML height is one of the challenging research topics in Korea and Japan. And there have been numerous evaluations (e.g., Betts *et al*. 1997) of the mixing depth predicted by regional models, but very few previous studies (e.g., Angevine and Mitchell 2001) which applied an estimate of ML height from wind profiler data to verify the ML height predicted by a NWP model. In the past, there was no objective technique to obtain the PBL depth observationally. The best way has been for a trained meteorologist to look over daily skew T-log P diagrams or time-height cross sections of different radar parameters, and use them to subjectively determine the PBL depth. Recent studies are trying to replace this time-consuming process by developing an objective technique such as, for example, using fuzzy logic techniques (Bianco and Wilczak 2002). But it still remains to statistically compare the subjective and objective techniques, and it will take some time to be readied for operational use. In this study, therefore, ML heights are estimated from the signal-to-noise ratio (SNR) data of KMA and JMA wind profiler sites. And these ML heights are utilized to qualitatively verify PBL heights predicted by the KMA regional numerical weather prediction model.

## 2. DATA AND METHOD

### 2.1 ***Principle***

The wind profilers observe Bragg scattering from the fluctuations in a refractive index produced by atmospheric turbulence. The fluctuations in the refractive index become large for some parts of the atmosphere, particularly in the regions where the vertical gradient of humidity is large and diffusion by turbulence is vigorous. In a ML that develops in daytime, diffusion by turbulence is intense and the vertical gradient of humidity is sharp at the top of the layer. Hence, the fluctuation in refractive index is likewise high at the top of the ML. Consequently, Bragg scattering is also strong at the top of the ML. The altitude where the maximum backscattered power is received by a wind profiler is regarded as the height of the ML top (Angevine *et al*. 1994). The ML height estimated by this method is known to correspond to the height from radiosonde and lidar observations (Angevine *et al*. 1994; Cohn and Angevine 2000). It is assumed in this paper that although a wind profiler observes scattering from fluctuations in the refractive index caused by eddies whose wavelength is 11 cm, half the profiler wavelength, this size of eddy exists within the various sized wavelengths of atmospheric turbulence. In a strict sense, there is no guarantee that 11 cm eddies are always present within a profiler's sampling volume. Frisch *et al.* (1986) addressed this question by using profilers operating at 50, 405, and 915 MHz. This well-known inner scale problem is one of the reasons that the U.S. National Weather Service wind profilers use the 449 MHz operating frequency, and is beyond the scope of this study.

Raw SNR varies depending on the distance between the antenna and a scatterer. Therefore, a distance correction should be added in order to make the raw SNR correspond directly to the fluctuation in refractive index. Corrected SNR (*SNRc,* dB) is derived using $SNRc = SNR + 20\log_{10}[(Z - Z_a)/Z_{st}]$, where *SNR*, *Z*, $Z_a$, and $Z_{st}$ are the raw signal-to-noise ratio (dB), altitude of a scatterer, antenna altitude, and normalization distance between a scatterer and an antenna, respectively. $Z_{st}$ is a constant standard distance, chosen appropriately for each profiler site.

## 2.2 *KMA wind profilers*

Table 1 shows the major features of wind profilers used in this study. The wave frequency of the KMA wind profiler is 1.29 GHz and its temporal resolution is 10 minutes. The KMA wind profilers have a vertical resolution of 70 m and first range gates at about 260 m, which makes them suitable for PBL depth measurement. The general data processing flow is divided into three steps. First, a fuzzy logic-based algorithm is applied to the incoming multiple peak data to identify the clear air signal. Second, a consensus algorithm is used on the identified clear air signal to reject outliers and the extract clear air signal as having a poor signal to noise ratio. Third, various quality control algorithms are used to ensure a reliable wind estimate.

### 2.2.1 Multi-peak

Selecting only one peak in the spectrum is not sufficient if atmospheric information is not the main feature in the spectrum. Consequently, we use several peaks in the power spectrum for each measurement gate (to consider wind, interference and noise). Dividing up the Doppler power spectrum into multiple regions/peaks is done statistically. Peaks having specific signatures (ground clutter, radio frequency interference, or point targets) are filtered from the spectra. The peaks are then recalculated before submitting the data to the multiple peak algorithm which identifies the most likely clear air peak. A fuzzy logic approach is used to choose the most likely clear air peak; Gaussian penalty functions are used. The peaks' scores depend on various spatial/temporal continuity criteria for velocity, spectral width, and power level. There are also various criteria which will reduce the score (i.e., ground clutter contamination or radio frequency interference). The peak with the highest score is kept and furnished to the consensus algorithm.

### 2.2.2 Consensus algorithm

For a given measurement direction, the consensus algorithm computes the most probable wind component. It proceeds by eliminating contaminated data and then averaging a set of peaks within a given velocity window. The processing applies a consensus algorithm over a user specified time window/period. It is applied in the following manner:

- data for a given direction of measurement (an antenna) and a gate of altitude is selected,
- the data is then screened for having a sufficient SNR,
- a sliding window of user specified width is applied to the Doppler (-V,+V) of the selected data,
- and the position of the window that maximizes the number of measurements present within the window is retained.

The representative value of the measurement (a projection of the wind in the processed/radar antenna direction) is the average of measurements present in the optimal window (in case of multi-peak data only the "best peak" is used). This value can still be rejected if it is considered to be inadequately representative of the measurement (if the optimal window does not contain enough measurements). In this case, it will be impossible to provide a wind vector corresponding to this altitude.

The processing parameters are:

- the period of measurements used to undertake the processing (field processing duration),
- the minimum acceptable SNR (field SNR Threshold (dB)),
- the width of the consensus window in meters per second (field width of the window),
- the minimum success rate: the percentage of measurements retained in the optimal window based on the total number of measurements in this same window (including measurements rejected for a signal to noise report that is too low) (field minimum success rate), and
- the minimum population: the minimum number of measurements used in the consensus (field minimum measurement number).

2.2.3 QUALITY CONTROL

The results of the consensus are then submitted to various quality control tests based on a statistical test. The radial consensus data are then combined to generate U, V, and W wind components. The vertical beam measurements are interpolated to the oblique beam heights if they differ. Missing data or data that have failed the statistical quality control are not replaced or interpolated and will cause missing data in the U, V, and W wind components. Within a melting layer, the interpolation of vertical components to same height as oblique components is very important in order not to introduce significant errors into the wind estimates. Quality can be temporal or spatial, associated with radial wind velocity, or associated with spectral width and/or with peak power. Temporal quality uses a reference profile (previous processing). Spatial quality uses a reference which is one of the measurement gates that is without interference and is determined dynamically for each spectrum.

**2.3 *JMA wind profilers***

The wave frequency of the JMA wind profiler is 1.36 GHz, which corresponds to a 22 cm wavelength. The available data are wind profiler SNRs whose observation interval is 10 minutes. The vertical resolution is about 300 m, the first range gate 394 m, and the upper limit of observable altitude from about 3 km (in winter) to 7 km (in summer). The SNR data passed through the signal processing and ordinary quality control for three dimensional wind speed. The quality control starts with the application of migrating-birds echo rejection and ground clutter rejection to the data. In the data processing stage, Doppler velocity is calculated. In the quality control stage, quadratic surface check and vertical shear check are applied to the data. In the data processing for the ML height calculation, the altitude where SNRc is a maximum is calculated for every 10-minute data interval. To eliminate unreasonable estimated heights for a mixed layer, the upper limit of the altitude is set to 3 km. Then estimated mixed layer heights can be obtained every 30 minutes from the median among the three temporal data samples (median is more appropriate than a simple average to prevent contamination by outliers) (Angevine *et al.* 1994).

**4. Qualitative evaluations of model-predicted ML heights**

It is crucial to verify the mixing depth predicted by a numerical prediction model not only for air quality forecasts but also for the improvement in the PBL scheme. Currently, the KMA global spectral and regional grid models use the NCAR CCM3 PBL (Holtslag and Boville 1993) and MRF PBL (Hong and Pan 1996) schemes, respectively, as the model vertical diffusion parameterizations (Lee *et al.* 2003). Both schemes are based on the non-local K-profile approach of Troen and Mahrt (1986), where the diagnosis of PBL height is an essential part of the parameterization (Beljaars 1992).

KMA wind profilers have lower first gate range and better vertical resolution than JMA profilers. Thus, in this section, we applied the SNRc from KMA wind profilers to evaluate model PBL heights. From the time series of vertical profiles of *SNRc*, the hourly the ML height information was obtained. Figure 2 shows an example of the effect from incorporating the distance correction. It can be seen that the temporal evolution of the ML height becomes clear after the distance correction is applied.

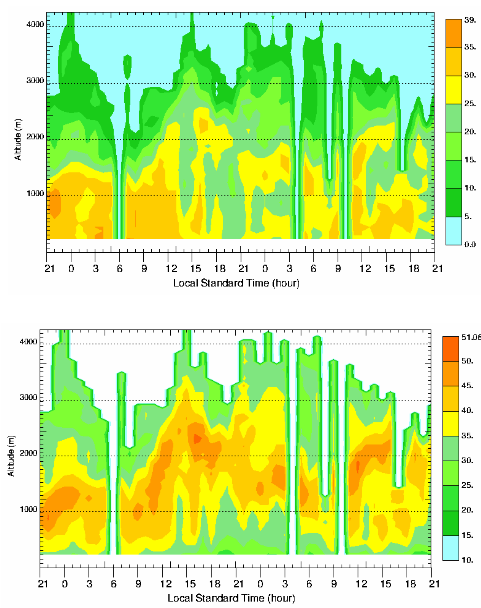


Figure 2. Temporal variation of the vertical profiles of SNR (unit: dB) data before (top) and after (bottom) distance correction.

**4.1** ***Numerical model and PBL scheme***

The operational NWP model used in this study is the Regional Data Assimilation and Prediction System (RDAPS), which is based on the MM5 mesoscale model developed by Pennsylvania State University (PSU) and the National Center for Atmospheric Research (NCAR). It runs twice a day for a 48-hour prediction and assimilates diverse observational data (Table 2). Figure 3 shows the model domains, which are composed of a 30 km mother domain and two nested domains for high-resolution (10 and 5 km) model runs.

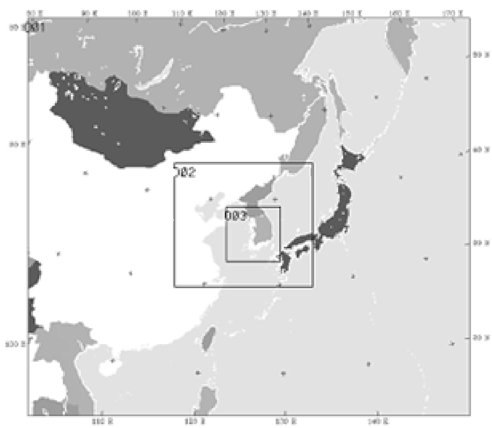

Figure 3. RDAPS model domains.

According to Hong and Pan (1996), PBL height of the KMA RDAPS is diagnosed by

$$h = Rib_{cr} \frac{\theta_{va} \, |U(h)|^2}{g(\theta_v(h) - \theta_s)},$$

where $Rib_{cr}$ is the critical bulk Richardson number, $\theta_s$ and $\theta_{va}$ are virtual potential temperatures near the model surface and at the lowest sigma level, respectively, $\theta_v(h)$ is the virtual potential temperature and $U(h)$ is the horizontal wind speed at height ($h$) of the PBL. This formula is known to represent downward flux well at the top of the PBL using two iterations. In the MRF PBL scheme, $h$ is defined not as the level for the inversion layer but as the level where the diffusivity becomes zero. At present, the RDAPS produces PBL height fields every 3 hours as one of the standard model output fields with a lead time of 48 hours.

**4.2** ***Qualitative comparison between observed and model-predicted mixing depths***

The model-predicted ML height is verified at observation points by comparing it with the ML height estimated from the SNR data from operational wind profiler observations. Precipitation or cloud in the boundary layer is an obstacle to the exact estimation of an ML height from wind profiler data, thus, close attention was paid to the their existence using high-resolution satellite and radar data. Figure 4 shows the sunshine percentage per day at Munsan and Gangneung in Korea from May to early September 2004. To select cases where a typical ML is developed in the high pressure region, we chose days with a lot of sunshine hours over 0.8 hour per hour. For sites in Japan, Kumagaya was selected for the analysis because this site showed clearer development of a mixed layer compared with other sites. The following three subsections describe the synoptic weather patterns for the selected cases using analyzed surface charts and satellite images (Figs. 5-8). And some qualitative comparison results are depicted for the cases using SNRc from wind profilers and ML heights from the KMA regional model (Figs. 9-12).

4.2.1 GANGNEUNG (31 AUG TO 3 SEP AND 18 TO 20 SEP 2004)

From 31 August to 3 September, the Gangneung area was influenced by a warm high-pressure system after typhoon CHABA passed by the Korean Peninsula before going away through the East Sea (Sea of Japan) as manifested in Fig. 5. The Gangneung area continued to exhibit clear skies. Figure 4 shows the sunshine rate at Gangneung and Munsan areas with a high sunshine percentage ranging from 70 to 80% during that period. Table 3 illustrates the sunshine hours from 30 Aug to 3 Sep 2004 with the hour bands of over 30 minutes shaded in gray. In Table 3, we can see the area kept almost 1.0 sunshine hours for each hour from sunrise to sunset on 1 to 2 September. The middle and low cloud amounts were small - below 10% (Table 4). Hence, a ML is well developed in the daytime.

Figure 9 shows temporal variations in the vertical profiles of SNR data from 1200 LST 30 Aug to 0900 LST 3 Sep 2004. The ML in which we are interested is the portion of the time series where the maximum value of SNR increased greatly with time from 0900 LST 1 September in Fig. 9b. The max SNR starts growing rapidly after sunrise and reached its peak of about 2 km. The peak corresponds to the top of the ML, which was predicted by the model almost exactly. Figure 9c shows the model-predicted ML heights after 12 hours. A second ML is developed. As well as with the previous day, the model predicted reasonably the observed two maximum heights of the two MLs. However, in Fig. 9d, the model overestimated the two maximum heights and predicted an early growth of the second ML by about one hour. This tendency appears to be more apparent in Fig. 10 where our center of attention is an ML developed on 20 Sep 2004 (Fig. 6).

On the other hand, Figure 9 shows two interesting features. One is the nocturnal maximum echo altitude and the other is the model ML height from 2100 LST 31 August to 0900 LST 1 September. These maximum echo altitudes correspond to the top of a RL. It is noticeable that a gradually descending RL top at night under a high pressure system is captured by the SNR data. The other is a coincidence between the maximum echo altitude and the model ML height (Figs. 9a and 9b, respectively). Basically, the model ML height can not represent the height of a RL because such kinds of diagnostic ML heights in the model can only stand for a ML with a hot surface, that is, a strongly convective boundary layer. Nevertheless, in this case, the model is thought to implicitly simulate the atmospheric situation at the top of a RL.

#### 4.2.2 MUNSAN (31 MAY 2004)

On 31 May 2004, Munsan was influenced by a high pressure system approaching from the northwest after the trough affected the Korean Peninsula (Fig. 6). On this day, the Munsan area showed a rapid increase in sunshine hours from 11.6 to 89% (Fig. 3). Average humidity was also lowered from 81.4 to 58.9%. Thus, this day had favorable atmospheric conditions for a well-developed ML in the high pressure region.

Figure 10 shows the SNR observation and model prediction results for ML height on this day. What we focus on in Fig. 11a is the portion where the max SNR begins to increase starting at 0900 LST on 31 May. For this ML, the model predicted its early growth (at about 1500 LST) and overestimated the maximum value of its height by several hundred meters. These characteristics of the model in predicting ML heights are repeated consistently in all four predictions. Another feature in Fig. 11 is a low ML height from 0900 to 1800 LST on 1 June. The model also seems to simulate this behavior fairly well although it still overestimates heights by about 500 m.

#### 4.2.3 KUMAGAYA (11 TO 13 AUG 2004)

During this period, Kumagaya in Japan is influenced by a North Pacific high pressure system and showed clear skies (Fig. 8). Figure 12 shows observations and model predictions of the ML height corresponding to this period. It can be seen that the MLs developed day after day starting from August 11. The wind profiler observations did not obviously show the growth and decay processes when compared with Korean wind profiler sites. That is mainly because Japan wind profiler observations have a vertical resolution of 300 m, which is much lower than 70 m of their Korea counterparts. Furthermore, it is also not suitable for resolving the top of the ML. This problem became more serious when 1 hour interval data were used. More frequent missing data also contributed to the failure to properly represent ML changes.

### 4.3 *Discussion*

The KMA wind profiler observations showed that a ML was more clearly developed under a warm high-pressure regime just after a trough or a tropical cyclone passage than during a series of sunny days. It seems to be because convective turbulence is generated vertically without environmental interruption in the former situation due to the scavenging effect of precipitation. Another possibility is that the difference in humidity between the ML and free atmosphere becomes too small for Bragg scattering because of the lower humidity in the ML after a long sequence of sunny days. Moreover, the existence of a RL may influence development of a ML. Because the ML develops by eroding an overlaid SBL gradually through their mutual boundary, it is possible that the cold air supply to the lower atmosphere due to a trough brings a base under which conditions a ML can clearly develop. When sunny days continue, a remaining RL may make the development of the ML ambiguous.

On the other hand, the evaluation of model-predicted ML heights against wind profiler SNR data at 10-minute intervals revealed the overall characteristics of the model PBL scheme. On the whole, the operational numerical model showed stable performance in capturing the features of the convective boundary layer situations. However, the model produced too early and too deep development of the ML as shown in Figs. 9d, 10, 11 and 12. The model's failure to reasonably predict could be attributed to the MRF PBL scheme's well known characteristics as pointed by

Noh *et al*. (2003). Excessively deep vertical mixing in the early phase of PBL growth, drying the lower PBL, is one of the commonly found problems in that scheme (Hong *et al*. 2003). Wind profiler SNR data at 1 hour intervals also evidently reflected the KMA model's deficiencies of having faster development with too high depth for a ML (not shown here).

## 5. SUMMARY AND DISCUSSION

ML height information is useful in observational and modeling studies of both air quality and NWP. In this study, ML heights are estimated from signal-to-noise ratio (SNR) data of wind profilers operated by KMA and JMA. The ML heights obtained are used to qualitatively verify mixing depth predicted by a KMA regional numerical weather prediction model.

The time-height cross sections of the SNR data exhibited evolution of a ML with great detail, even with a gradually descending RL top at night. In particular, Korea wind profilers showed the development of a ML more evidently than Japanese profilers. At the same temporal resolution of 1 hour, the one grasped more easily the growth of a ML than the other due to its vertical resolution, which is 4 times finer (not shown here). Japanese profilers have a 100 m vertical resolution mode. Thus, a lot of valuable information, including the influence of geographical conditions, can be gathered if the 100 m resolution mode becomes operational.

The comparison between wind profiler data and the model results can contribute to the diagnosis of the problems in numerical models. It is suggested in this paper that the ML height estimated from wind profiler SNR data can be employed as an auxiliary tool for evaluating the KMA regional model ML height forecasts on an operational basis. Especially, wind profiler SNR data is expected to help diagnose problems that a model PBL scheme has in operational runs and improve it. Also, the incorporation of additional information, such as vertical velocity and spectral width (Heo *et al*. 2003), would make the estimation of ML height more exact.

Ordinary radiosonde observations have limitations in evaluating rapidly changing ML heights due to their poor temporal resolution. From the operational viewpoint, therefore, we have no real-time and high-resolution observations available for model ML height verifications. Until newer and more stable methods come out, for the time being the wind profiler SNR data could be used limitedly in the case of clear skies for the operational evaluation of KMA model mixing depth forecasts. And to make this kind of approach a routine part of model evaluation, a longer period of study will be carried out.

## ACKNOWLEDGEMENTS

The authors would like to thank Drs. Wayne M. Angevine and James M. Wilczak for their helpful comments. We also thank Mary Hart for proofread.

## REFERENCES

Angevine, W. M., A. B. White, and S. K. Avery, 1994: Boundary-layer depth and entrainment zone characterization with a boundary-layer profiler. *Bound.-Layer Meteor.*, **68**, 375-385.

_______________, H. K. Baltink, and F. C. Bosveld, 2001: Observations of the morning transition of the convective boundary layer. *Bound.-Layer Meteor.*, **101**, 209-227.

Angevine, W. M., and K. Mitchell, 2001: Evaluation of the NCEP mesoscale Eta model convective boundary layer for air quality applications. *Mon. Wea. Rev.,* **129**, 2761-2775.

Arya, S. P., 1988: *Introduction to Micro-Meteorology*. Academic Press, Orlando, FL, 307 pp.

Beljaars, A., 1992: The parameterization of the planetary boundary layer. Meteorological Training Course Lecture Series, European Center for Medium-Range Weather Forecasts, 57 pp.

Betts, A. K., F. Chen, K. E. Mitchell, and Z. I. Janji, 1997: Assessment of the land surface and boundary layer models in two operational versions of the NCEP Eta model using FIFE data. *Mon. Wea. Rev.*, **125**, 2896-2916.

Bianco, L., and J. M. Wilczak, 2002: Convective boundary layer depth: Improved measurement by Doppler radar wind profiler using fuzzy logic method. *J. Atmos. Oceanic Technol.*, **19**, 1745-1758.

Campistron, B., S. Bernard, B. Benech, F. Ardhuin-Giraid, J. Dessens, E. Dupont, and B. Carissimo, 2002: Turbulent dissipiation rate in the boundary layer via UHF wind profiler

Doppler spectral width measurements. *Bound.-Layer Meteor.*, **103**, 361-389.

Cohn, S. A., and W. M. Angevine, 2000: Boundary layer height and entrainment zone thickness measured by lidars and wind-profiling radars. *J. Appl. Meteor.*, **39**, 1233-1247.

Gupta, S., R. T. McNider, M. Trainer, R. J. Zamora, K. Knupp and M. P. Singh, 1997: Nocturnal wind structure and plume growth rates due to inertial oscillations. *J. Appl. Meteor.,* **36**, 1050-1063.

Heo, B.-H., S. Jacoby-Koaly, K.-E. Kim, B. Campistron, B. Benech, and E.-S. Jung, 2003: Use of the Doppler spectral width to improve the estimation of the convective boundary layer height from UHF wind profiler observations. *J. Atmos. Oceanic Technol.*, **20**, 408-424.

Holtslag, A. A. M., and B. A. Boville, 1993: Local versus nonlocal boundary layer diffusion in a global climate model. *J. Climate*, **6**, 1825-1842.

Hong, S.-Y., and H.-L. Pan, 1996: Nonlocal boundary layer vertical diffusion in a medium-range forecast model. *Mon. Wea. Rev.*, **124**, 2322-2339.

__________, and _________, 1998: Convective trigger function for mass-flux cumulus parameterization scheme. *Mon. Wea. Rev*., **126**, 2599-2620.

__________, J. Dudhia, and Y. Noh, 2003: A new vertical diffusion package with explicit treatment of the entrainment processes. *Proc. International Workshop on NWP Models for Heavy Precipitation in Asia and Pacific Areas*, Tokyo, Japan, Japan Meteorological Agency. [Available online at http://pfi.kishou.go.jp/open/ws0302e.htm.]

Kawai, H., 2002: Forecast of sulfur dioxide flow from Miyake Volcano with a high resolution regional transport model. CAS/JSC WGNE Research Activities in Atmospheric and Oceanic Modeling, **32**, 0524-0525, WMO/TD-No. 1105.

Kobayashi, T., 1995: Studies on wind profiler techniques for the measurements of winds. Technical Reports of the Meteorological Research Institute, Meteorological Research Institute, No. 35, 8-24. (in Japanese)

Lee, S.-J., H. Park, D.-K. Rha, and J.-Y. Cho, 2003: The NWP system on operation and the plan for heavy rain prediction at KMA. *Proc. International Workshop on NWP Models for Heavy Precipitation in Asia and Pacific Areas*, Tokyo, Japan, Japan Meteorologial Ageny. [Available online at http://pfi.kishou.go.jp/open/ws0302e.htm.]

Lemone, M. A., M. Zhou, C.-H. Moeng, D. H. Lenschow, L. J. Miller, and R. L. Grossman, 1999: An observational study of wind profiles in the baroclinic convective mixed layer. *Bound.-Layer Meteor.*, **90**, 47-82.

Marsik, F. J., K. W. Fischer, T. D. McDonald, and P. J. Samson, 1995: Comparison of methods for estimating mixing height used during the 1992 Atlanta field intensive. *J. Appl. Meteor.*, **34**, 1802-1814.

Nagai, H., H. Terada, and M. Chino, 2001: Relation between nasty smell at Kanto area on 28 Aug 2000 and eruption at Miyake Island: Examination by numerical simulation. *Tenki*, **48**, 227-230. (in Japanese)

Niisoe, T., and H. Kida, 2000: A three-dimensional chemistry transport model analysis of sulfur cycle in polluted air. Disaster Prevention Research Institute Annuals, Kyoto University, No.43 B-1, 229-235. (in Japanese)

Noh, Y., W.-G. Cheon, and S.-Y. Hong, 2003: Improvement of the K-profile model for the planetary boundary layer based on large eddy simulation data. *Bound.-Layer Meteor.*, **107**, 401-427.

Rogers, R. R., W. L. Ecklund, D. A. Carter, K. S. Gage, and S. A. Ethier, 1993: Research applications of a boundary-layer wind profiler. *Bull. Amer. Meteor. Soc*., **74**, 567-580.

Stull, R. B., 1988: *An Introduction to Boundary Layer Meteorology*. Kluwer Academic, 666 pp.

Troen, I., and L. Mahrt, 1986: A simple model of the atmospheric boundary layer: Sensitivity to surface evaporation. *Bound.-Layer Meteor*., **37**, 129-148.

Yi, C., K. J. Davis, and B. W. Berger, 2001: Long-term observations of the dynamics of the continental planetary boundary layer. *J. Atmos. Sci*., **58**, 1288-1299.

Table 1. Major characteristics of wind profilers and their data used in this study.

| Site | latitude longitude | sea level altitude | minimum range gate | frequency | dz | dt |
|---|---|---|---|---|---|---|
| Munsan (47099) | 37˚ 52' 126˚ 46' | 31 m | 261 m | 1.29 GHz | 70 m | 10 min |
| Gangneung (47105) | 37˚ 46' 128˚ 52' | 33 m | 263 m | 1.29 GHz | 70 m | 10 min |
| Kumagaya (47626) | 36˚ 09' 139˚ 22' | 30 m | 394 m | 1.36 GHz | 300 m | 10 min |

Table 2. Major specification of operational RDAPS at KMA.

| | regional model | high-resolution model | |
|---|---|---|---|
| dynamics | nonhydrostatic | | |
| grid interval | 30 km | 10 km | 5 km |
| dimension | 171×191 | 160×178 | 141×141 |
| time steps | 60 sec | 30 sec | 15 sec |
| forecast time | 48 hrs | 24 hrs | |
| Initialization | FDDA (12 hr) | 3h-cycle (IAU) | 1-way interaction |
| lateral boundary condition | relaxation | time and inflow/outflow dependent relaxation | |
| explicit moisture | mixed phase (water vapor, cloud, rain, ice, snow) | | |
| deep convection | Kain-Fritch scheme | | none |
| PBL | Non-local MRF-PBL scheme | | |
| ground temperature | 5-layer soil model | | |
| radiation | cloud radiation | | |

Table 3. Sunshine hour for each hour in Gangneung from 30 Aug to 3 Sep 2004.

| | 6h | 7h | 8h | 9h | 10h | 11h | 12h | 13h | 14h | 15h | 16h | 17h | 18h | 19h | sum |
|---|---|---|---|---|---|---|---|---|---|---|---|---|---|---|---|
| 30 Aug | 0.0 | 0.0 | 0.0 | 0.0 | 0.0 | 0.0 | 0.0 | 0.0 | 0.0 | 0.0 | 0.0 | 0.0 | 0.0 | 0.0 | 0.0 |
| 31 Aug | 0.0 | 0.4 | 0.9 | 1.0 | 1.0 | 1.0 | 1.0 | 1.0 | 1.0 | 0.9 | 1.0 | 1.0 | 0.8 | 0.0 | 11.0 |
| 1 Sep | 0.0 | 0.0 | 0.0 | 0.5 | 1.0 | 1.0 | 0.9 | 1.0 | 1.0 | 0.6 | 1.0 | 1.0 | 1.0 | 0.2 | 9.2 |
| 2 Sep | 0.0 | 0.4 | 0.9 | 1.0 | 1.0 | 1.0 | 1.0 | 1.0 | 1.0 | 1.0 | 1.0 | 1.0 | 1.0 | 0.2 | 11.5 |
| 3 Sep | 0.0 | 0.0 | 0.4 | 1.0 | 1.0 | 0.9 | 1.0 | 1.0 | 0.5 | 0.4 | 0.3 | 0.0 | 0.6 | 0.0 | 7.1 |

Table 4. As in Table 3, but for middle and low cloud amount.

| | 3h | 6h | 9h | 12h | 15h | 18h | 21h | 24h | mean |
|---|---|---|---|---|---|---|---|---|---|
| 30 Aug | 4 | 3 | 5 | 5 | 6 | 6 | 10 | 10 | 6.1 |
| 31 Aug | 2 | 0 | 0 | 0 | 0 | 0 | 2 | 2 | 0.8 |
| 1 Sep | 3 | 1 | 2 | 3 | 3 | 0 | 0 | 0 | 1.5 |
| 2 Sep | 0 | 0 | 1 | 1 | 2 | 1 | 0 | 0 | 0.6 |
| 3 Sep | 0 | 0 | 0 | 0 | 1 | 3 | 4 | 3 | 1.4 |

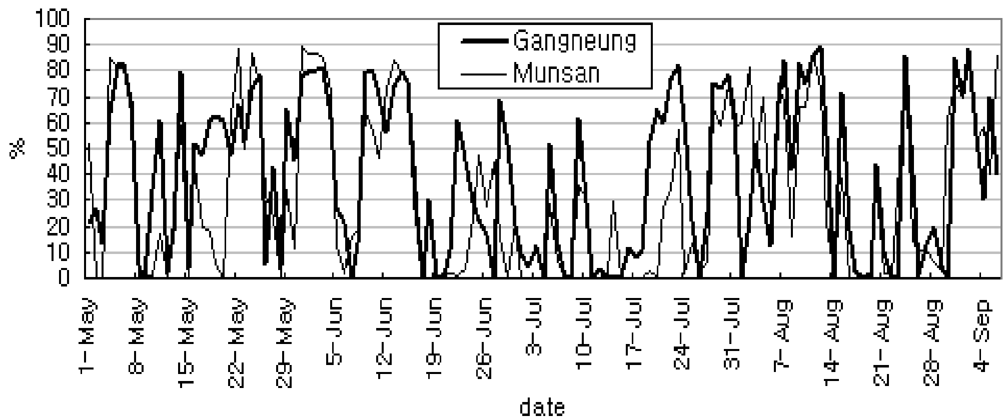


Figure 4. Sunshine (%/day) at Gangneung and Munsan wind profiler sites from 1 May to 5 Sep 2004.

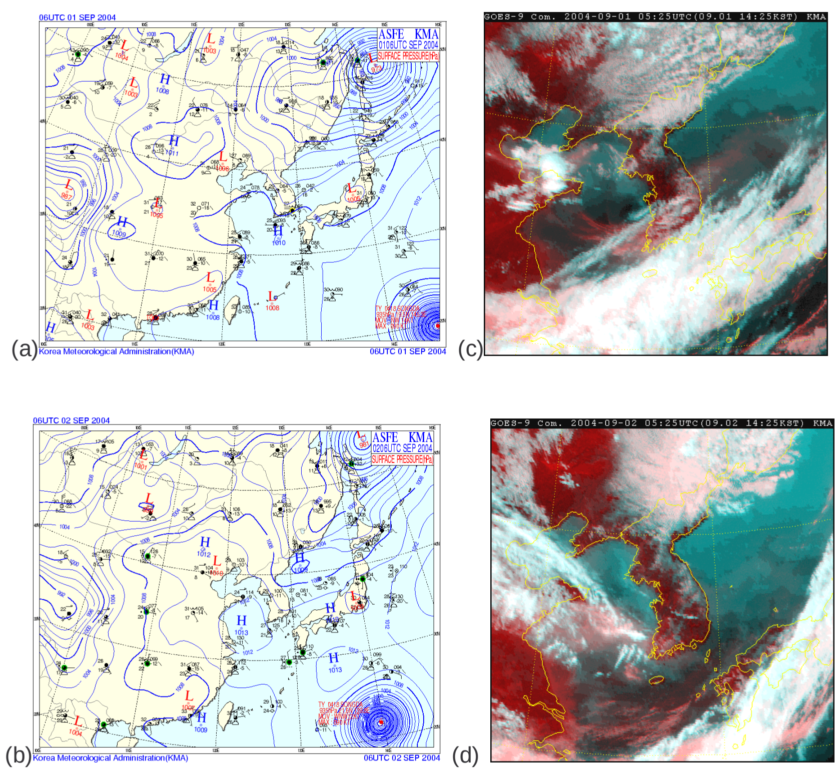


Figure 5. Surface weather charts at 0600 UTC (a) 1 & (b) 2 Sep and GOES Satellite composite images at 0525 UTC (c) 1 & (d) 2 Sep 2004.

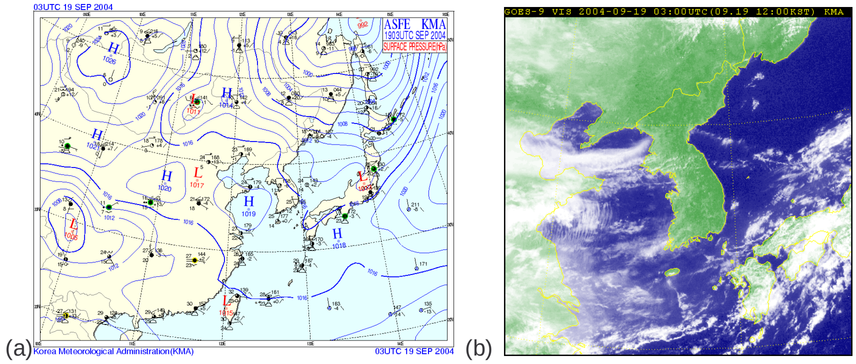


Figure 6. (a) Surface weather chart and (b) GOES satellite composite image at 0300 UTC 19 Sep 2004.

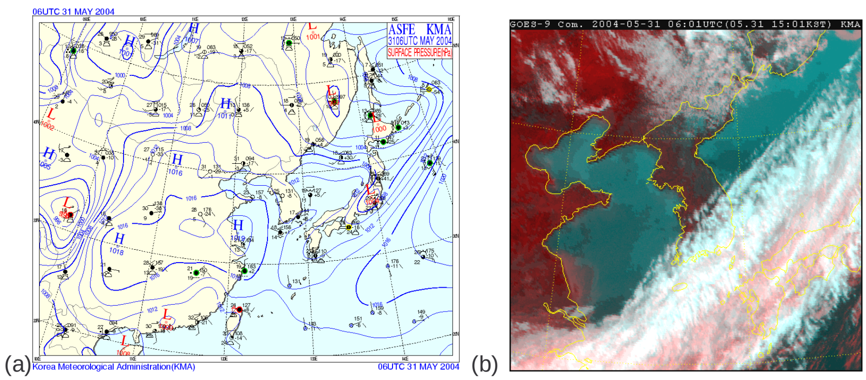


Figure 7. (a) Surface weather chart and (b) GOES satellite composite image at 0600 UTC 31 May 2004.

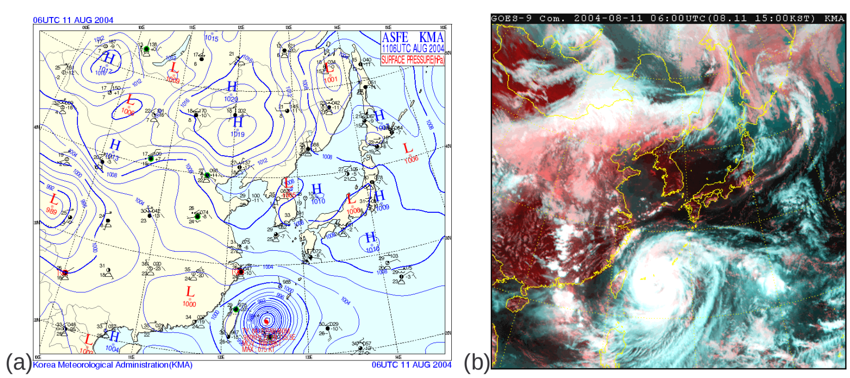


Figure 8. (a) Surface weather chart and (b) GOES satellite composite image at 0600 UTC 11 Aug 2004.

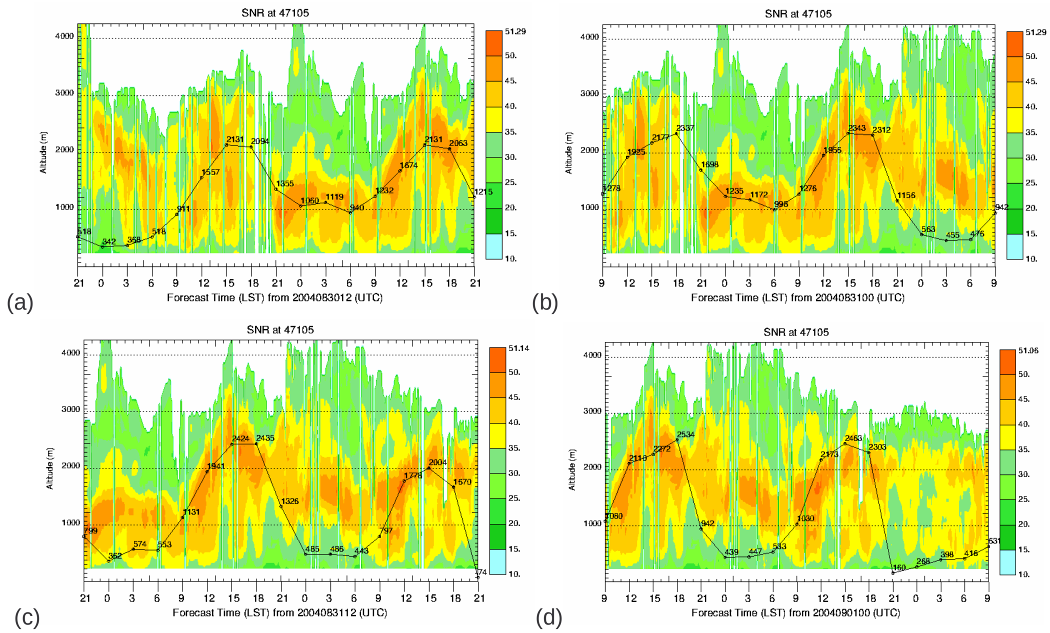


Figure 9. The verification of the model-predicted mixed layer height by SNR data of the ind profiler. Solid lines are diurnal variations of PBL height predicted by the operational regional model (30 km) with initial time (a) 1200 UTC 30 Aug, (b) 0000 UTC 31 Aug, (c) 1200 UTC 31 Aug, and (d) 0000 UTC 1 Sep 2004. The color-filled contours are distance-corrected SNR fields at Gangneung(47105) wind profiler.

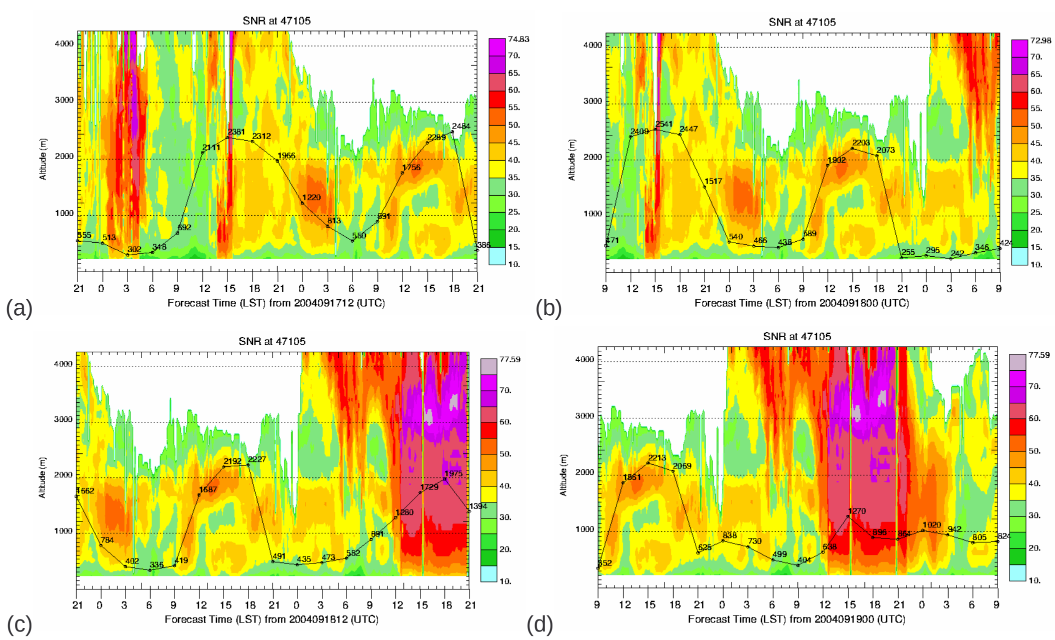


Figure 10. As in Fig. 9, but from 18 to 20 Sep 2004.

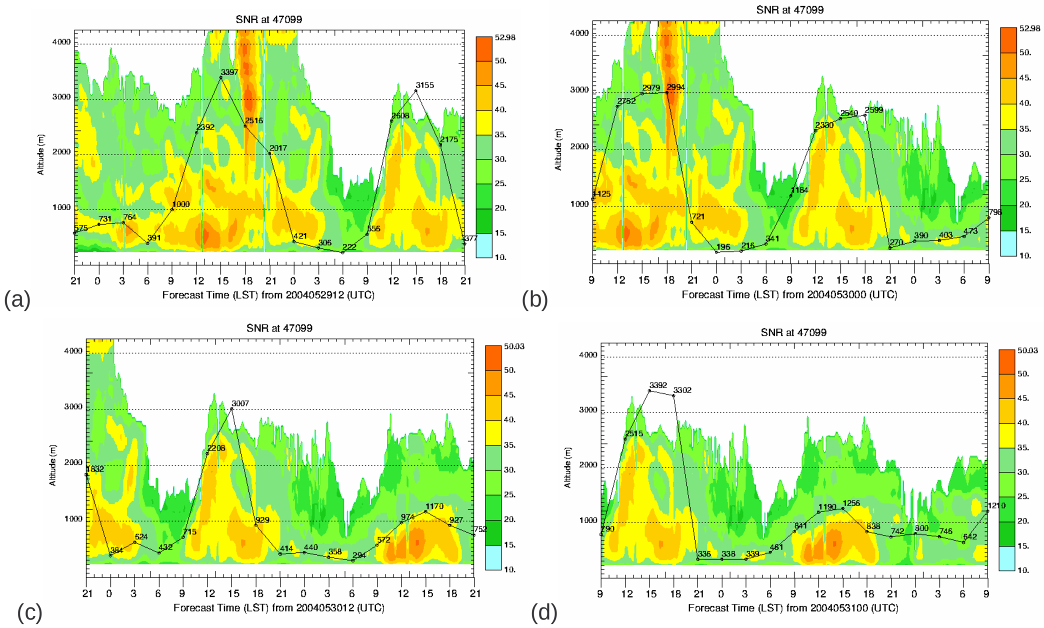


Figure 11. As in Fig. 9, but for Munsan(47099) from 29 to 31 May 2004.

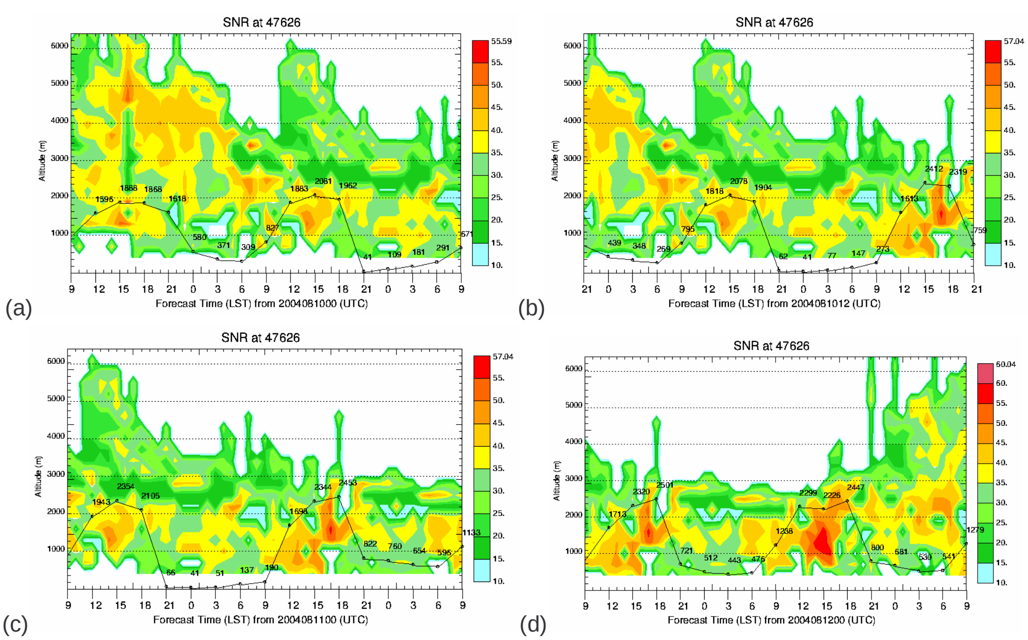


Figure 12. As in Fig. 9, but for Kumagaya(47626) from 10 to 13 Aug 2004.